Herpes simplex virus type 1 interaction with myeloid cells *in vivo*

Maitreyi Shivkumar[1,3], Clara Lawler[2], Ricardo Milho[1,4], Philip G. Stevenson[1,2,5]

[1]Division of Virology, Department of Pathology, University of Cambridge, UK

[2]School of Chemistry and Molecular Biosciences, University of Queensland and Royal Children's Hospital, Brisbane, Australia.

[3]Current address: Division of Infection and Immunity, University College London, London, UK

[4]Current address: Costello Medical Consulting, Cambridge, UK

[5]Correspondence to: Dr. P.G. Stevenson, Level 4 Building 76, School of Chemistry and Molecular Biosciences, University of Queensland, St Lucia, Brisbane, Queensland 4072, Australia. tel. +61-7-3636-1614; fax. +61-7-3636-1401; email p.stevenson@uq.edu.au

Abstract

Herpes simplex virus type 1 (HSV-1) enters mice via olfactory epithelial cells, then colonizes the trigeminal ganglia (TG). Most TG nerve endings are subepithelial, so this colonization implies subepithelial viral spread, where myeloid cells provide an important line of defence. The outcome of myeloid cell infection by HSV-1 *in vitro* depends on their differentiation state; the outcome *in vivo* is unknown. Epithelial HSV-1 commonly infected myeloid cells, and cre-lox virus marking showed nose and lung infections passing through $lysM^+$ and $CD11c^+$ cells. By contrast subcapsular sinus macrophages (SSM) exposed to lymph-borne HSV-1 were permissive only when type 1 interferon (IFN-I) signaling was blocked; normally their infection was suppressed. Thus the myeloid infection outcome helped to determine HSV-1 distribution: subepithelial myeloid cells provided a route of spread from the olfactory epithelium to TG neurons, while SSM blocked systemic spread.

Journal of Virology JVI Journal of Virology

28 **Importance**

29 Herpes simplex virus type 1 (HSV-1) infects most people and can cause severe disease. This
30 reflects its persistence in nerve cells that connect to the mouth, nose, eye and face.
31 Established infection seems impossible to clear. Therefore we must understand how it
32 starts. This is hard in humans, but mice show HSV-1 entry via the nose then spread to its
33 preferred nerve cells. We show that this spread proceeds in part via myeloid cells, which
34 normally function in host defence. Myeloid infection was productive in some settings, but
35 was efficiently suppressed by interferon in others. Therefore interferon acting on myeloid
36 cells can stop HSV-1 spread and enhancing this defence offers a way to improve infection
37 control.

38

39

Introduction

The α-, β- and γ-herpesviruses establish broadly neuro-, myelo- and lymphotropic persistent infections (1). Less is known about acute infection, as sporadic transmission and late clinical presentation make it hard to analyse. Acutely adaptive immunity exerts little restraint on viral tropism, so common themes are likely. The difficulty of clearing established infections makes these themes important to understand. Genomic comparisons indicate that herpesvirus infections long pre-date human speciation (2). Therefore related mammalian herpesviruses are likely to share mechanisms of host colonization, allowing those of experimentally tractable hosts to provide new insights. Murid herpesviruses have particular value in this regard, as their hosts provide the main *in vivo* experimental model of mammalian biology.

Murid Herpesvirus-4 (MuHV-4, a gamma-herpesvirus), Murine cytomegalovirus (MCMV, a beta-herpesvirus) and HSV-1 (an alpha-herpesvirus) all enter mice via olfactory neurons (3-5). MuHV-4 and MCMV spread thence to lymph nodes (LN) (4, 6), while HSV-1 spreads to the TG (5). Nonetheless each virus penetrates the epithelium and so will encounter subepithelial myeloid cells. While these normally provide an early defence against invading pathogens, MCMV exploits them to spread (7) and persist (8), and MuHV-4 exploits them to reach B cells (9). How HSV-1 interacts with myeloid cells is less well understood.

Ex vivo human blood-derived monocytes resist productive HSV-1 infection, but become susceptible after culture (10). Murine macrophages are similar (11, 12). Human monocyte-derived dendritic cells (DC) support productive infection when immature and lose susceptibility with maturation (13). Again murine DC appear to be similar (14). MCMV (8) and HCMV (15) establish latent infections of myeloid cells that are reactivated by

maturation signals (8). MuHV-4 also establishes latency in myeloid cells (16), but with a strong tendency to lytic reactivation. It inhibits myeloid cell functions extensively when lytic, and minimally when latent (17). HSV-1 also impairs myeloid cell functions (18), causing host shutoff even when infection is abortive (19). Herpesvirus infections remain immunogenic because uninfected cells can engage in cross-priming. Therefore the purpose of viral evasion in infected myeloid cells is probably to delay their recognition (20, 21). For MCMV and MuHV-4 this makes sense, as they use myeloid infection to reach other cell types. The relevance for HSV-1 is less clear.

Myeloid cell depletions increase murine susceptibility to HSV-1-induced disease (22, 23), presumably because uninfected myeloid cells protect via immune priming and type I interferon (IFN-I) production (24-26). Infected myeloid cells might also promote anti-viral responses. However how *in vitro* myeloid cell phenotypes relate to those encountered *in vivo* is hard to know. A fundamental question is whether *in vivo* myeloid cell infection is productive. Key contexts are when incoming virions first encounter subepithelial myeloid cells, and when infection spreads to the myeloid sentinels of lymph nodes (LN). We show by cre-mediated genetic marking that HSV-1 can pass productively through the subepithelial myeloid cells of infected mice. LN myeloid cells contrastingly restricted infection, unless IFN-I signalling was blocked.

Materials and Methods

Mice C57BL/6J (Animal Resources Centre, Perth, Australia; or Harlan Ltd, Oxford, UK), CD11c-Cre (27) and LysM-cre mice (28) were maintained at University of Queensland or University of Cambridge animal units and infected when 6–12 weeks old. Experiments were approved by the University of Queensland Animal Ethics Committee in accordance with Australian National Health and Medical Research Council guidelines (project 301/13), and by the University of Cambridge ethical review board and the UK Home Office under the 1986 Animal (Scientific Procedures) Act (Project 80/2538). For nasal infections, virus (10^6 p.f.u. in 5µl) was pipetted onto the nares of mice held prone under light restraint without anesthesia, and was spontaneously inhaled (29). For lung infections, mice were anesthetised with isoflurane and virus (10^6 p.f.u.) was inhaled in 30µl. For whisker pad infections, mice were anesthetised with isoflurane, virus (10^6 p.f.u. in 20µl) was applied to each whisker pad, and 20 scratches were made through each drop with a 27 gauge needle. Ear pinna infections were similarly by scarification under anesthesia, applying virus (10^6 p.f.u. in 20µl) to the left ear pinna and making 20 scratches made through the drop. Footpad infections (10^6 p.f.u. in 50µl) were by injection under isoflurane anesthesia. To deplete NK cells, mice were injected intraperitoneally (i.p.) with 200µg purified mAb PK136 (anti-NK1.1, Bio-X-cell), 1 and 3 days before infection and every 2 days thereafter. Cell depletion was >90% effective, as measured by flow cytometry of spleen cells with an antibody to NKp46. To block IFN-I responses we have mice i.p. 200µg purified mAb MAR1-5A3 (Bio-X-Cell), 1 day before infection and every 2 days thereafter. This mAb binds to the IFN-I receptor (IFNAR) and prevents IFN-I binding. Experimental groups were compared statistically by Student's 2 tailed unpaired t test.

Cells Macrophages were recovered by post-mortem peritoneal lavage, followed by removal of non-adherent cells. They were >90% F4/80$^+$ by immunostaining. Embryonic fibroblasts were harvested from day 13-14 mouse embryos by trypsin digestion and gentle tissue grinding. These cells, BHK-21 fibroblasts (American Type Culture Collection (ATCC) CCL-10), NIH-3T3-cre fibroblasts (30), RAW-264 monocyte / macrophages (ATCC TIB-71), K562 myeloid leukemia cells (ATCC CCL-243), THP-1 monocytes (ATCC TIB-202), and U937 histiocytic lymphoma cells (ATCC CRL-1593) were grown in Dulbecco's modified Eagle's medium supplemented with 2mM glutamine, 100IU/ml penicillin, 100µg/ml streptomycin and 10% fetal calf serum (complete medium).

Viruses MHV-RG is a derivative of MuHV-4 with a viral M3 (lytic) promoter between the 3' ends of ORFs 57 and 58 driving loxP-flanked mCherry upstream of GFP (9). MHV-RG expresses mCherry, but loxP site recombination by cre excises the mCherry coding sequence, switching the virus irreversibly to GFP expression from the same promoter (MHV-G). We used HSV-1 strain SC16 (31). The HSV-GFP derivative has an HCMV IE1 promoter transcribing GFP from the US5 locus (5). To make HSV-RG, the loxP-mCherry-pA-loxP-GFP construct of MHV-RG was amplified with *Pfu* polymerase (Promega Corporation), adding *Hin*DIII and *Bam*HI restriction sites to its respective 5' and 3' ends. The PCR product was cloned into the same sites of pcDNA3 (Invitrogen Corporation), then sub-cloned into pHD5-CRE (32) using an *Spe*I restriction site in the HCMV IE1 promoter, and *Xho*I sites in the pcDNA3 polylinker and downstream of the cre coding sequence in pHD5-CRE. Thus, HCMV IE1-loxP-mCherry-pA-loxP-GFP-pA was inserted into US5 (genomic site 137945, Genbank X14112). The plasmid was linearised with *Sca*I and co-transfected with HSV-1 SC16 viral DNA into BHK-21 cells using Fugene-6 (Roche Diagnostics). MCherry$^+$ virus was identified under

ultraviolet illumination, enriched by flow cytometric sorting of infected cells, and plaque-purified by limiting dilution. We derived switched HSV-RG (HSV-G) by passage in NIH-3T3-cre cells and limiting dilution cloning in BHK-21 cells. All viruses were checked by sequence across the US5 insertion site and by restriction enzyme mapping of viral DNA. Virus stocks were grown in BHK-21 cells (5). Virus was recovered from infected cells and supernatants by ultracentrifugation (38,000 x *g*, 90min). The pelleted cells were sonicated to break up aggregates then stored in aliquots at -80^{o}C.

Virus assays Virus stocks, cells and organ homogenates were titered for infectivity by plaque assay. Virus dilutions were incubated with BHK-21 cell monolayers (37^{o}C, 2h), overlaid with complete medium plus 0.3% carboxymethylcellulose and cultured at 37^{o}C. After 2 days (HSV-1) or 4 days (MuHV-4) the monolayers were fixed in 4% formaldehyde and stained with 0.1% toluidine blue. Plaques were counted under x30 microscopy. To measure both pre-formed infectious and reactivatable MuHV-4, freshly isolated PLN or spleen cell suspensions were co-cultured with BHK-21 cells for 4 days and plaques detected as above. To measure both pre-formed infectious and reactivatable HSV-1, TG were disrupted gently, then incubated (37^{o}C, 30min) with Liberase TL (2WU/ml) and DNase I (0.2mg/ml) (Roche Diagnostics). The released cells were plated on BHK-21 cell monolayers and cultured for 2 days before fixation, staining and plaque counting. Viral fluorochrome switching was determined by plaque or infectious centre assay at limiting dilution in 96-well plates (16 wells per dilution). After 2 days (HSV-1) or 4 days (MuHV-4), wells were scored under UV illumination for green (GFP^{+}, switched) and red (mCherry^{+}, unswitched) fluorescence to derive titers for each. We calculated % switching as 100 x green titer/(red titer + green titer).

156

157 **Immunostaining of tissue sections** Organs were fixed in 1% formaldehyde /
158 10mM sodium periodate / 75mM L-lysine (18h, 4°C). Noses were decalcified by gentle
159 agitation in 150mM NaCl / 50mM TrisCl (pH=7.2) / 270mM EDTA for two weeks at 23°C,
160 changing the solution every 2-3 days. All tissues were then equilibrated in 30% sucrose (24h,
161 4°C) and frozen in OCT. Sections (6µm) were air-dried (1h, 23°C), washed 3x in PBS, blocked
162 with 0.3% Triton X-100 / 5% normal donkey serum (1h, 23°C), then incubated (18h, 4°C) with
163 combinations of primary antibodies to: GFP (rabbit pAb or goat pAb, AbCam), B220 (rat
164 monoclonal Ab (mAb) RA3-6B2, Santa Cruz Biotechnology), CD68 (rat mAb FA-11, AbCam),
165 α-tubulin (rat mAb YL1/2, Serotec), βIII-tubulin (mouse mAb TU-20, AbCam), CD31 (rat mAb
166 ER-MP12, Serotec), F4/80 (rat mAb CI:A3–1, Santa Cruz Biotechnology), mCherry (rabbit
167 pAb, Badrilla), CD169 (rat mAb 3D6.112, Serotec), and polyclonal rabbit sera to MuHV-4
168 (raised in-house by x3 subcutaneous virus inoculation) and HSV-1 (rabbit pAb, either from
169 Sigma Chemical Co or raised in house by immunizing rabbits subcutaneously x3 with HSV-1
170 SC16). After incubation, sections were washed 3× in PBS, incubated (1h, 23°C) with
171 combinations of Alexa568 or Alexa647-donkey anti-rat IgG pAb, Alexa488- or Alexa568-
172 donkey anti rabbit IgG pAb (Life Technologies), and Alexa488-donkey anti-goat pAb
173 (Abcam), then washed 3× in PBS, counterstained with DAPI and mounted in Prolong Gold
174 (Life Technologies). Fluorescence was visualized with Zeiss LSM 510/710 or Leica TCS SP2
175 confocal microscopes, or a Nikon epifluorescence microscope, and analyzed with Zen
176 imaging software or ImageJ.

177

178 **Immunofluorescence of cells** Cells were seeded on glass coverslips then infected and
179 18h later fixed in 2% paraformaldehyde / PBS, permeabilized in 0.1% Triton X-100, blocked

with 5% goat serum, and incubated with rabbit anti-HSV-1 pAb followed by Alexa488-conjugated goat anti-rabbit pAb (Invitrogen). Cellular actin was stained with TRITC-conjugated phalloidin (Sigma Chemical Co). Nuclei were stained with DAPI. Cells were mounted in Prolong Gold (Invitrogen) and imaged on a Leica TCS SP2 confocal microscope.

Flow cytometry Fibroblasts were trypsinized, washed in PBS and analyzed on a FACSCalibur (BD Biosciences). MCherry and GFP fluorescence were visualized directly. To identify NK cells, dissociated spleen cells were blocked with anti-CD16/32 (BD Biosciences), incubated with biotinylated anti-NKp46 mAb (Biolegend) then Alexa488-conjugated streptavidin (Invitrogen), then washed x2 in PBS and analysed on a FACS Calibur (BD Biosciences).

Immunoblotting Cells were lysed (4^{o}C, 30min) in 1% Triton X-100, 50 mM TrisCl pH=7.4, 150 mM NaCl, with Complete protease inhibitors (Roche Diagnostics). Cell debris and nuclei were removed by centrifugation (13,000 x g, 15 min). Lysates were heated to 70˚C in Laemmli's buffer, followed by SDS-PAGE and electrophoretic transfer to nitrocellulose membranes. Blots were probed with mouse mAbs CB24 to gB (33) and LP1 to VP16 (34) and developed with rabbit anti-mouse IgG pAb and LI-COR imaging.

Results

HSV-1 infects myeloid cells at its likely natural entry site

Most experimental HSV-1 infections are initiated by scarification. Natural infection is more likely to occur at an intact mucosal surface. HSV-1 fails to infect non-scarified mice orally but infects them nasally via olfactory neurons (5). Nasal infection showed extensive sub-epithelial spread (Fig.1a). Epithelial infection was always present, and early infection is solely epithelial (5), but sub-epithelial infection evidently spread faster. Myeloid cells ($CD68^+$) were abundantly recruited to subepithelial infection sites, whether from primary olfactory infection or secondary spread to the respiratory epithelium (Fig.1b). Many of these infiltrating cells expressed viral lytic antigens (Fig.1c). Therefore HSV-1 commonly infected subepithelial myeloid cells after mucosal host entry.

HSV-1 strain SC16 replicates in RAW-264 monocyte / macrophages

HSV-1 strain SC16, a low passage isolate derived in the 1970s, was used to establish anti-viral chemotherapy (35) and a glycoprotein H-deficient vaccine (36). Its tropism for myeloid cells has not been tested. It replicated in RAW-264 monocyte / macrophages (Fig.2a). Productive infection was validated by immunoblotting for the virion gB and VP16 (Fig.2b). However RAW-264 cells produced fewer infectious virions than BHK-21 fibroblasts (Fig.2a), and after overnight infection (3 p.f.u. / cell), 16.8% of RAW-264 cells expressed viral lytic antigens (Fig.2c), whereas >99% of BHK-21 cells did so (data not shown). Three human myeloid cell lines - K562, THP-1 and U937 - supported productive infection even less well than RAW-264 cells (Fig.2a). Therefore SC16 was similar to other HSV-1 strains in showing a modest capacity to replicate in myeloid cells *in vitro*.

HSV-RG allows cell-type specific virus tracking

Viral lytic gene expression in CD68$^+$ cells (Fig.1) suggested productive myeloid infection. To track this functionally we generated a floxed reporter virus HSV-RG, inserting in the non-essential US5 locus (37) a human CMV IE1 promoter driving a floxed mCherry coding sequence plus poly-A site, upstream of a GFP coding sequence plus poly-A site (Fig.3a). HSV-RG expressed mCherry (red fluorescence), until mCherry excision by cre irreversibly switched its fluorochrome expression to GFP (green) (Fig.3b). The unswitched HSV-RG and switched HSV-G showed no difference in replication in cre$^+$ or cre$^-$ cells *in vitro* (Fig.3c). Both showed minor *in vivo* attenuation after nasal inoculation relative to the parental HSV-1 SC16 wild-type, presumably due to US5 disruption, but no defect relative to each-other (Fig.3d). Therefore HSV-RG provided a tool capable of unbiased viral tracking through cre$^+$ cells.

HSV-RG is recombined by lysM-cre mice

A cellular path connects each recovered virion to host entry. Virus tagging tells us what proportion of productive paths traversed a cre$^+$ cell. LysM-cre mice express cre mainly in neutrophils, mature macrophages (28, 38, 39), and type 2 alveolar epithelial cells (40). HSV-RG accordingly showed fluorochrome switching in peritoneal macrophages but not embryonic fibroblasts of lysM-cre mice (Fig.4a). We compared lung infection by HSV-RG with MuHV-4 carrying a similar switching cassette (MHV-RG) (Fig.4b, 4c). Gr1$^+$ neutrophils and inflammatory monocytes cells entering the lungs do not express lysM (40); and neither MuHV-4 nor HSV-1 infects type 2 alveolar epithelial cells (41). Thus at least acutely, viral fluorochrome switching could be interpreted as replication in alveolar macrophages. MuHV-4 enters the lungs via alveolar macrophages (40) and MHV-RG accordingly showed

248 substantial switching after 1 day. HSV-1 infects mainly type 1 alveolar epithelial cells (40)
249 but also showed substantial switching at days 1 and 2 post-inoculation.

250 Herpesviruses given nasally (i.n.) also infect the upper respiratory tract (29).
251 Therefore we assayed also the fluorochrome expression of HSV-RG and MHV-RG recovered
252 from noses (Fig.4c). Upper respiratory tract infection proceeds more slowly than lung
253 infection, so we sampled the mice at day 3. HSV-RG and MHV-RG were both less switched in
254 noses than in lungs, so fewer virions followed paths through lysM^{+} cells, but switching was
255 detectable nonetheless.

256 Nasal HSV-1 spreads to the trigeminal ganglia (TG) after 2-3 days and re-emerges in
257 the facial skin after 4-5 days (5). Thus, virions in the TG should be at least as switched as
258 those in noses, and those in the skin should be at least as switched as those in the TG. After
259 lung plus nose infection (large inoculation volume with anesthesia), the HSV-RG recovered
260 from TG or skin at day 4 was similarly switched to that from noses. Selective upper
261 respiratory tract infection (low volume inoculation without anesthesia) also showed no
262 significant differences in switching between HSV-RG from noses, TG and skin (Fig.4e).
263 Therefore productive myeloid cell infection occurred early, *en route* from the olfactory
264 epithelium to the TG. Immunostaining of tissue sections identified mCherry^{+} and GFP^{+}
265 infected cells in the TG (Fig.4f) and in the superficial layers of the skin (Fig.4g). Thus, virus re-
266 emerging from the TG possibly avoids exposure to lysM^{+} cells because it re-emerges in the
267 epidermis (5).

268 Inoculation of the whisker pad or the ear pinna by scarification, routes commonly
269 used for experimental HSV-1 infection, gave less switching (Fig.4h). This reflected possibly
270 that scarification provides direct access to sub-epithelial nerve endings, bypassing the
271 normal myeloid cell defences of intact epithelia.

HSV-RG is recombined by CD11c-cre mice

Myeloid cells are highly diverse. No single promoter identifies them all or defines exclusive sub-populations (42). Thus to back-up the results with lysM-cre mice, we tracked HSV-RG fluorochrome switching in CD11c-cre mice. Immunostaining shows CD11c expression in DC and some macrophage populations, including lymph node (LN) subcapsular sinus macrophages (SSM) (43). Few DC express lysM (28). Thus, CD11c and lysM expression identify partly overlapping populations, with CD11c-cre mice measuring HSV-1 passage through more DC-type myeloid cells.

As in lysM-cre mice, HSV-RG was more switched in CD11c-cre lungs than in noses, although switching was detectable in both sites (Fig.5a). A direct comparison of CD11c-cre and LysM-cre i.n. infections at day 4 (Fig.5b) showed somewhat more switching in CD11c-cre mice for both noses and TG. Each transgenic showed more switching in noses than in TG. This was statistically significant for CD11c-cre mice but not for LysM-cre. Analysing larger numbers of i.n.-infected CD11c-cre mice at day 5 (Fig.5c) confirmed greater switching in noses than in TG.

Type I interferons (IFN-I) restrict HSV-1 infection of myeloid cells

Viral fluorochrome switching is irreversible, and so should increase cumulatively between infection sites. Thus, the decrease in HSV-RG switching from noses to TG indicated that although $CD11c^+$ cells generated new virions, they passed infection to neurons less well than $CD11c^-$ cells. Switched and unswitched viruses had equal fitness, so this result suggested that replication in $CD11c^+$ cells carried an extra cost, for example due to innate immune stimulation. $CD11c^+$ cells readily pass MuHV-4 to LN (6, 9). By contrast HSV-1 lung

296 and nose infections gave <50 p.f.u. per LN (data not shown). HSV-1 may lack the capacity to
297 exploit DC migration. However virions should still reach LN via the lymph. Therefore we
298 considered that $CD11c^+$ cell infection might inhibit HSV-1 propagation by local immune
299 activation, for example by eliciting IFN-I, which has anti-HSV-1 activity in both humans and
300 mice (44-46). The LN subcapsular sinus is a prominent site of IFN-I responses (47), and
301 Herpes virions inoculated into footpads (i.f.) directly reach $CD11c^+$ subcapsular sinus
302 macrophages (SSM) (39, 43). Therefore to test *in vivo* how IFN-I affected HSV-1 myeloid cell
303 infection, we gave mice i.p. anti-IFNAR antibody or not, then i.f. GFP^+ HSV-1 (Fig.6).

304 At 1 day post-inoculation, IFNAR blockade had no significant effect on HSV-1 titers in
305 footpads but increased substantially titers in the popliteal LN (PLN) (Fig.6a). By day 3, IFNAR
306 blockade had increased footpad titers, PLN titers remained elevated, and infection had
307 spread to the liver and spleen (Fig.6b), implying passage from the PLN to the blood.
308 Immunostaining PLN sections at day 1 (Fig.6c, 6d) showed significantly more viral GFP^+ and
309 viral $antigen^+$ cells around the subcapsular sinus after IFNAR blockade. Both viral markers
310 co-localized with CD68 and CD169, indicating SSM infection. The few infected cells of
311 control mice also included examples of co-localization with CD68 and CD169. By day 3
312 substantial inflammatory infiltrate into the PLN of IFNAR-blocked mice was evident by $CD68^+$
313 staining (Fig.6e, compare Fig.6d). CD169 expression was largely lost but expression of the
314 tissue macrophage marker F4/80, which SSM lack (48), was increased, and both $CD68^+$ and
315 $F4/80^+$ cells were HSV-1 $antigen^+$. $B220^+$ B cells and $CD31^+$ vascular endothelial cells showed
316 no infection. Therefore IFNAR blockade increased HSV-1 infection specifically in SSM and
317 other myeloid cells.

318 One action of IFN-I at the subcapsular sinus is NK cell recruitment (49). To test
319 whether this could account for the protection of SSMs against HSV-1 by IFN-I, we compared

IFNAR blockade with NK1.1$^+$ cell depletion in C57Bl/6 mice. NK cell depletion significantly increased day 1 PLN virus titers (Fig.6f). However IFNAR blockade increased them more, and while IFNAR blockade increased viral GFP$^+$ cell numbers on PLN sections, NK cell depletion did not have a significant effect. Therefore NK cells contributed to anti-HSV-1 defence at the subcapsular sinus but could not account for most IFN-I-dependent protection. The strong anti-viral efficacy of IFN-I at day 1, with inhibition of both viral reporter and lytic gene expression, suggested that it acted directly on SSM to block infection at a very early stage.

Site-specific changes in HSV-RG switching in IFNAR-blocked mice

We tested next whether IFNAR blockade increased HSV-1 production by myeloid cells, as measured by fluorochrome switching (Fig.7). IFNAR blockade increased day 3 lung virus titers in lysM-cre mice (Fig.7a). However the recovered virus showed no increase in switching. As virus titers were higher, more switched virus was produced, but IFNAR blockade evidently also increased lysM$^-$ cell virus production. Total virus titers also increased in lysM-cre noses and footpads without increasing the fraction switched (Fig.7b, 7c).

In TG (Fig.7b), total titers and switching both increased. Therefore IFN-I limited macrophage-dependent passage to the TG more than macrophage-independent passage, although the proportion of virus that was switched remained low, so passage through lysM$^+$ cells to the TG was still an accessory route. By contrast LN virus showed abundant switching in IFNAR-blocked mice, comparable to that of lungs. LN infection was too low to assess switching in control mice, but the substantial rise in virus titers and high level of switching after IFNAR blockade implied copious virus production by lysM$^+$ cells, most likely SSM (Fig.6).

343 IFNAR blockade of CD11c-cre mice gave similar results: it increased HSV-RG titers in
344 lungs, noses and footpads without significantly increasing switching; it increased both titers
345 and switching in TG; and it increased LN titers with abundant switching. Thus, IFN-I
346 regulated HSV-1 spread to a degree determined by myeloid cell involvement. In LN, it
347 protected SSM and so blocked viraemic spread. In subepithelial tissues it also moderated
348 myeloid infection but did not prevent myeloid cell-independent virus passage from the
349 olfactory epithelium to the TG. Fig.8 outlines our understanding of how myeloid cell
350 infection fits into the HSV-1 lifecycle.
351

352 **Discussion**

353 Sentinel macrophages and DC monitor tissues for normal senescence and for
354 pathogen invasion. They are particularly numerous below epithelial surfaces and where
355 extracellular fluid enters LN. Thus despite the anatomical restriction of HSV-1 persistence to
356 local neuronal ganglia, subepithelial spread after mucosal entry led it to myeloid cells.
357 Comparison with other herpesviruses that enter via the olfactory epithelium (3, 4) reveals
358 myeloid infection as a common theme, providing access to diverse latency reservoirs.

359 The different outcomes of HSV-1, MuHV-4 and MCMV myeloid infections can be
360 explained in part by the tendency of each virus to initiate lytic or latent gene expression.
361 MCMV must remain latent in monocytes to reach secondary infection sites such as the
362 salivary glands; MuHV-4 must remain latent in DC until they contact B cells; each reactivates
363 presumably in response to microenvironmental signals reaching the myeloid cell nucleus.
364 HSV-1 has a superficially simpler host colonization strategy of replicating lytically until it
365 enters a neuron. Its tendency to lytic replication and capacity to infect many cell types make
366 innate immune defences key to preventing acute disease. IFNAR blockade greatly increased
367 virus titers, consistent with what is observed in $IFNAR^{-/-}$ mice (45). The fluorochrome
368 switching of TG virus in lysM-cre and CD11c-cre mice indicated that myeloid cells intercept
369 some of the HSV-1 penetrating the olfactory epithelium, and through IFN-I hinder its spread
370 to trigeminal neurons; but the key role of IFN-I was in LN, where its protection of SSM
371 prevented systemic infection.

372 SSM do not form a physical barrier to lymph-borne virus spread, as they merely stud
373 the subcapsular sinus wall (50). Rather they adsorb viruses from the lymph (51). This
374 sampling allows SSMs to initiate early innate and adaptive immune responses. Cumulative
375 virion adsorption along the tortuous lymphatic channels of serial LN also stops lymph-borne

376 virions reaching the blood. The lymph cleansing depends on SSM not supporting replication
377 of viruses they adsorb, or at least slowing their replication sufficiently for immune responses
378 to become effective. The importance here of IFN-I was evident from IFNAR blockade
379 allowing HSV-1 to replicate in SSM and to reach the liver and spleen, consistent with viremic
380 spread.

381 SSM also limit the spread of MuHV-4 and MCMV (39, 43). MuHV-4 bypasses this
382 restriction by entering LN in DC. The route MCMV takes is yet to be defined, but it is clearly
383 more permissive than SSM. HSV-1 was able to pass through upper and lower respiratory
384 tract myeloid cells but not through SSM. As VSV can replicate in SSM (51) it is unclear why
385 herpesviruses have not evolved to do so. HSV-1 IFN-I evasion (52) may be more complete in
386 humans than in mice. However the restriction of clinical HSV-1 lesions to a trigeminal
387 distribution argues that human LN are also an effective barrier to spread. As HSV-1 still
388 reached neurons when IFN-I signalling was intact, there may be limited selective pressure
389 for more complete evasion. TG infection increased without IFN-I, but viral evolution is
390 driven by transmission efficiency whether greater initial HSV-1 delivery to neurons increases
391 long-term shedding is uncertain. Viral re-emergence from TG neurons is more directly
392 relevant to transmission. Thus it was of interest that HSV-1 passage from TG to skin seemed
393 to avoid lysM^{+} cells, perhaps because most skin infection is epidermal (5). Excessive IFN-I
394 evasion may have down-sides: IFN-I contributes to the homeostasis of immune cells (53)
395 and possibly also neurons (54), so complete blockade might compromise persistence in
396 these cell types. Such compromises forced on persistent viruses provide potential means of
397 improving infection control.
398

References

1. **Fenner F, White DO.** 1994. Medical Virology 4th edition. Academic Press.

2. **McGeoch DJ, Rixon FJ, Davison AJ.** 2006. Topics in herpesvirus genomics and evolution. Virus Res **117:**90-104.

3. **Milho R, Frederico B, Efstathiou S, Stevenson PG.** 2012. A heparan-dependent herpesvirus targets the olfactory neuroepithelium for host entry. PLoS Pathog **8:**e1002986.

4. **Farrell HE, Lawler C, Tan CS, MacDonald K, Bruce K, Mach M, Davis-Poynter N, Stevenson PG.** 2016. Murine Cytomegalovirus Exploits Olfaction To Enter New Hosts. MBio **7:**e00251-16.

5. **Shivkumar M, Milho R, May JS, Nicoll MP, Efstathiou S, Stevenson PG.** 2013. Herpes simplex virus 1 targets the murine olfactory neuroepithelium for host entry. J Virol **87:**10477-10488.

6. **Gaspar M, May JS, Sukla S, Frederico B, Gill MB, Smith CM, Belz GT, Stevenson PG.** 2011. Murid herpesvirus-4 exploits dendritic cells to infect B cells. PLoS Pathog **7:**e1002346.

7. **Stoddart CA, Cardin RD, Boname JM, Manning WC, Abenes GB, Mocarski ES.** 1994. Peripheral blood mononuclear phagocytes mediate dissemination of murine cytomegalovirus. J Virol **68:**6243-6253.

8. **Brautigam AR, Dutko FJ, Olding LB, Oldstone MB.** 1979. Pathogenesis of murine cytomegalovirus infection: the macrophage as a permissive cell for cytomegalovirus infection, replication and latency. J Gen Virol **44:**349-359.

9. **Frederico B, Milho R, May JS, Gillet L, Stevenson PG**. 2012. Myeloid infection links epithelial and B cell tropisms of Murid Herpesvirus-4. PLoS Pathog **8:**e1002935.

10. **Linnavuori K, Hovi T.** 1981. Herpes simplex virus infection in human monocyte cultures: dose-dependent inhibition of monocyte differentiation resulting in abortive infection. J Gen Virol **52:**381-385.

11. **Stevens JG, Cook ML.** 1971. Restriction of herpes simplex virus by macrophages. An analysis of the cell-virus interaction. J Exp Med **133:**19-38.

12. **Lopez C, Dudas G.** 1979. Replication of herpes simplex virus type 1 in macrophages from resistant and susceptible mice. Infect Immun **23:**432-437.

13. **Kobelt D, Lechmann M, Steinkasserer A.** 2003. The interaction between dendritic cells and herpes simplex virus-1. Curr Top Microbiol Immunol **276:**145-161.

14. **Jones CA, Fernandez M, Herc K, Bosnjak L, Miranda-Saksena M, Boadle RA, Cunningham A.** 2003. Herpes simplex virus type 2 induces rapid cell death and functional impairment of murine dendritic cells in vitro. J Virol **77:**11139-11149.

15. **Taylor-Wiedeman J, Sissons P, Sinclair J.** 1994. Induction of endogenous human cytomegalovirus gene expression after differentiation of monocytes from healthy carriers. J Virol **68:**1597-1604.

16. **Weck KE, Kim SS, Virgin HW, Speck SH.** 1999. Macrophages are the major reservoir of latent murine gammaherpesvirus 68 in peritoneal cells. J Virol **73:**3273-3283.

17. **Rosa GT, Gillet L, Smith CM, de Lima BD, Stevenson PG.** 2007. IgG fc receptors provide an alternative infection route for murine gamma-herpesvirus-68. PLoS One **2:**e560.

18. **Salio M, Cella M, Suter M, Lanzavecchia A.** 1999. Inhibition of dendritic cell maturation by herpes simplex virus. Eur J Immunol **29:**3245-3253.

19. **Samady L, Costigliola E, MacCormac L, McGrath Y, Cleverley S, Lilley CE, Smith J, Latchman DS, Chain B, Coffin RS.** 2003. Deletion of the virion host shutoff protein (vhs)

444 from herpes simplex virus (HSV) relieves the viral block to dendritic cell activation: potential
445 of vhs- HSV vectors for dendritic cell-mediated immunotherapy. J Virol **77:**3768-3776.
446 20. **Smith CM, Gill MB, May JS, Stevenson PG.** 2007. Murine gammaherpesvirus-68 inhibits
447 antigen presentation by dendritic cells. PLoS One **2:**e1048.
448 21. **Mount AM, Masson F, Kupresanin F, Smith CM, May JS, van Rooijen N,Stevenson**
449 **PG, Belz GT.** 2010. Interference with dendritic cell populations limits early antigen
450 presentation in chronic γ-herpesvirus-68 infection. J Immunol **185:**3669-3676.
451 22. **Zisman B, Hirsch MS, Allison AC.** 1970. Selective effects of anti-macrophage serum,
452 silica and anti-lymphocyte serum on pathogenesis of herpes virus infection of young adult
453 mice. J Immunol **104:**1155-1159.
454 23. **Kassim SH, Rajasagi NK, Zhao X, Chervenak R, Jennings SR.** 2006. In vivo ablation
455 of CD11c-positive dendritic cells increases susceptibility to herpes simplex virus type 1
456 infection and diminishes NK and T-cell responses. J Virol **80:**3985-3993.
457 24. **Linnavuori K, Hovi T.** 1983. Restricted replication of herpes simplex virus in human
458 monocyte cultures: role of interferon. Virology **130:**1-9.
459 25. **Domke I, Straub P, Kirchner H.** 1986. Effect of interferon on replication of herpes
460 simplex virus types 1 and 2 in human macrophages. J Virol **60:**37-42.
461 26. **Brücher J, Domke I, Schröder CH, Kirchner H.** 1984. Experimental infection of inbred
462 mice with herpes simplex virus VI: effect of interferon on in vitro replication in
463 macrophages. Arch Virol **82:**83-93.
464 27. **Caton ML, Smith-Raska MR, Reizis B.** 2007. Notch-RBP-J signaling controls the
465 homeostasis of CD8- dendritic cells in the spleen. J Exp Med **204:**1653-1664.
466 28. **Clausen BE, Burkhardt C, Reith W, Renkawitz R, Förster I.** 1999. Conditional gene
467 targeting in macrophages and granulocytes using LysMcre mice. Transgenic Res **8:**265-277.

468 29. **Tan CS, Frederico B, Stevenson PG.** 2014. Herpesvirus delivery to the murine respiratory
469 tract. J Virol Methods **206:**105-114.
470 30. **Stevenson PG, May JS, Smith XG, Marques S, Adler H, Koszinowski UH, Simas JP,**
471 **Efstathiou S.** 2002. K3-mediated evasion of CD8+ T cells aids amplification of a latent
472 gamma-herpesvirus. Nat Immunol **3:**733-740.
473 31. **Hill TJ, Field HJ, Blyth WA.** 1975. Acute and recurrent infection with herpes simplex virus
474 in the mouse: a model for studying latency and recurrent disease. J Gen Virol **28:**341-353.
475 32. **Proença JT, Coleman HM, Connor V, Winton DJ, Efstathiou S.** 2008. A historical analysis
476 of herpes simplex virus promoter activation in vivo reveals distinct populations of latently
477 infected neurones J Gen Virol **89:**2965–2974.
478 33. **Zenner HL, Yoshimura S, Barr FA, Crump CM.** 2011. Analysis of Rab GTPase-activating
479 proteins indicates that Rab1a/b and Rab43 are important for herpes simplex virus 1
480 secondary envelopment. J Virol **85:**8012–8021.
481 34. **McLean C, Buckmaster A, Hancock D, Buchan A, Fuller A, Minson A.** 1982. Monoclonal
482 antibodies to three non-glycosylated antigens of herpes simplex virus type 2. J Gen Virol
483 **63:**297-305.
484 35. **Field HJ, Darby G, Wildy P.** 1980. Isolation and characterization of acyclovir-resistant
485 mutants of herpes simplex virus. J Gen Virol **49:**115-124.
486 36. **Farrell HE, McLean CS, Harley C, Efstathiou S, Inglis S, Minson AC.** 1994. Vaccine
487 potential of a herpes simplex virus type 1 mutant with an essential glycoprotein deleted. J
488 Virol **68:**927-932.
489 37. **Balan P, Davis-Poynter N, Bell S, Atkinson H, Browne H, Minson T.** 1994. An analysis of
490 the in vitro and in vivo phenotypes of mutants of herpes simplex virus type 1 lacking
491 glycoproteins gG, gE, gI or the putative gJ. J Gen Virol **75:**1245-1258.

492 38. **Frederico B, Chao B, May JS, Belz GT, Stevenson PG.** 2014. A murid gamma-
493 herpesviruses exploits normal splenic immune communication routes for systemic spread.
494 Cell Host Microbe **15:**457-470.
495 39. **Frederico B, Chao B, Lawler C, May JS, Stevenson PG.** 2015. Subcapsular sinus
496 macrophages limit acute gammaherpesvirus dissemination. J Gen Virol **96:**2314-2327.
497 40. **Lawler C, Milho R, May JS, Stevenson PG.** 2015. Rhadinovirus host entry by co-operative
498 infection. PLoS Pathog **11:**e1004761.
499 41. **Farrell HE, Lawler C, Oliveira MT, Davis-Poynter N, Stevenson PG.** 2015. Alveolar
500 Macrophages Are a Prominent but Nonessential Target for Murine Cytomegalovirus
501 Infecting the Lungs. J Virol **90:**2756-2766.
502 42. **Hume DA.** 2011. Applications of myeloid-specific promoters in transgenic mice support
503 in vivo imaging and functional genomics but do not support the concept of distinct
504 macrophage and dendritic cell lineages or roles in immunity. J Leukoc Biol **89:**525-538.
505 43. **Farrell HE, Davis-Poynter N, Bruce K, Lawler C, Dolken L, Mach M, Stevenson PG.** 2015.
506 Lymph Node Macrophages Restrict Murine Cytomegalovirus Dissemination. J Virol **89:**7147-
507 7158.
508 44. **Sancho-Shimizu V, Perez de Diego R, Jouanguy E, Zhang SY, Casanova JL.** 2011. Inborn
509 errors of anti-viral interferon immunity in humans. Curr Opin Virol **1:**487-496.
510 45. **Luker GD, Prior JL, Song J, Pica CM, Leib DA.** 2003. Bioluminescence imaging reveals
511 systemic dissemination of herpes simplex virus type 1 in the absence of interferon
512 receptors. J Virol **77:**11082-11093.
513 46. **Rosato PC, Leib DA.** 2015. Neuronal Interferon Signaling Is Required for Protection
514 against Herpes Simplex Virus Replication and Pathogenesis. PLoS Pathog **11:**e1005028.

515 47. **Sandberg K, Eloranta ML, Campbell IL.** 1994. Expression of alpha/beta interferons (IFN-
516 alpha/beta) and their relationship to IFN-alpha/beta-induced genes in lymphocytic
517 choriomeningitis. J Virol **68:**7358–7366.
518 48. **Gray EE, Cyster JG.** 2012. Lymph node macrophages. J Innate Immun **4:**424-436.
519 49. **Garcia Z, Lemaître F, van Rooijen N, Albert ML, Levy Y, Schwartz O, Bousso P.** 2012.
520 Subcapsular sinus macrophages promote NK cell accumulation and activation in response to
521 lymph-borne viral particles. Blood **120:**4744-4750.
522 50. **Anderson AO, Shaw S.** 1993. T cell adhesion to endothelium: the FRC conduit system
523 and other anatomic and molecular features which facilitate the adhesion cascade in lymph
524 node. Semin Immunol **5:**271-282.
525 51. **Kuka M, Iannacone M.** 2014. The role of lymph node sinus macrophages in host
526 defense. Ann N Y Acad Sci **1319:**38-46.
527 52. **Paladino P, Mossman KL.** 2009. Mechanisms employed by herpes simplex virus 1 to
528 inhibit the interferon response. J Interferon Cytokine Res **29:**599-607.
529 53. **Mattei F, Schiavoni G, Tough DF.** 2010. Regulation of immune cell homeostasis by type
530 I interferons. Cytokine Growth Factor Rev **21:**227-236.
531 54. **Reyes-Vázquez C, Prieto-Gómez B, Dafny N.** 2012. Interferon modulates central nervous
532 system function. Brain Res **1442:**76-89.
533

Acknowledgements

We thank Stacey Efstathiou and lab members for advice, Colin Crump for mAb CB24 and Susanne Bell for mAb LP1. MS was supported by a Medical Research Council UK studentship. The work was also supported by the BBSRC (BB/J014419/1), the Australian Research Council (FT130100138), the Australian National Health and Medical Research Council (project grants 1064015, 1060138 and 1079180), and by Belspo (collaborative grant BelVir).

Figure legends

Figure 1. Myeloid cell infection by nasally inoculated HSV-1.

a. Mice were given HSV-1 SC16 i.n. (10^6 p.f.u. in 5µl). After 3 days, nose sections were stained for HSV-1 antigens, for α-tubulin to identify olfactory neurons and their apical cilia, and with DAPI to identify cell nuclei. The boxed region in the upper panel is shown at higher magnification below. The images are representative of more than 10 mice.

b. Mice were infected as in **a**. After 3 days, nose sections were stained for HSV-1 antigens, CD68 (macrophages / DC) and with DAPI (cell nuclei). Examples are shown of a primary olfactory epithelial infection site and a secondary respiratory epithelial infection site, both with extensive overlap between viral antigen expression and $CD68^+$ myeloid cell infiltration. The images are representative of 6 mice examined.

c. Mice were infected as in **a**. After 1 day nose sections were stained for HSV-1 antigens and for CD68 as in **b**. 3 examples of neuroepithelial infection are shown. Arrows show example $CD68^+HSV\text{-}1^+$ cells. The right-hand panels show the boxed areas in more detail.

Figure 2. Myeloid cell infection by HSV-1 SC16 *in vitro*.

a. BHK-21 fibroblasts, murine RAW-264 monocyte / macrophages, and human myeloid cell lines (K562, THP-1, U937) were infected with HSV-1 (3 p.f.u. / cell, 1h) then washed in pH = 3 buffer to inactivate remaining extracellular virions and cultured at 37°C (t=0). 3, 8, 18 and 24h later, replicate cultures were assayed for infectivity by plaque assay. Mean ± SD of 2 experiments are shown. BHK-21 cells produced significantly more virus than RAW-264 cells, and they produced significantly more virus than the human cell lines.

563 **b.** Cells were infected as in **a**, then lysed, electrophoresed and immunoblotted for the viral
564 gB (mAb CB24), VP16 (mAb LP1) and cellular actin. The left lane shows molecular weight
565 markers.
566 **c.** RAW-264 cells were infected as in **a** or left uninfected, cultured (24h, 37^{o}C), fixed,
567 permeabilized and stained for HSV-1 antigens with a polyclonal serum. Actin was stained
568 with phalloidin-TRITC and nuclei with DAPI. Of >1000 cells counted, 16.8% were viral
569 antigen^{+}.
570
571 **Figure 3. Characterization of floxed colour switching HSV-1 (HSV-RG).**
572 **a.** We inserted into the non-essential HSV-1 US5 locus an expression cassette comprising an
573 HCMV IE1 promoter, a floxed mCherry coding sequence plus poly A site, and a GFP coding
574 sequence plus poly A site. LoxP recombination by cre removed the mCherry coding
575 sequence plus poly A site, switching viral fluorochrome expression from red to green.
576 **b.** NIH-3T3-cre cells were accordingly green by epifluorescence microscopy when infected
577 by HSV-RG (0.01 p.f.u. / cell, 24h), whereas infected cre^{-} BHK-21 cells were red.
578 **c.** BHK-21 and NIH-3T3-cre cells were infected (0.01 p.f.u. / cell, 2h) with unswitched (HSV-
579 RG) or switched virus (HSV-G), then washed in pH=3 buffer and cultured in complete
580 medium. Time = 0 is when virus was added. At each time point replicate cultures were
581 assayed for red and green fluorescent infectivity by overnight infection of BHK-21 cells in
582 the presence of phosphonoacetic acid (100µg/ml) to limit infection to a single cycle, and
583 flow cytometric enumeration of red and green BHK-21 cells. Each point corresponds to
584 10,000 cells counted. The data show similar growth of HSV-RG and HSV-G in both cell lines
585 and almost complete switching of HSV-RG in NIH-3T3-cre cells.

586 **d.** C57BL/6 mice were infected i.n. (10^6 p.f.u. in 5µl without anesthesia) with HSV-RG, HSV-G
587 or wild-type HSV-1 SC16. 3 or 5 days later, tissues were assayed for infectious virus by
588 plaque assay. All HSV-RG plaques were red and all HSV-G plaques were green. SC16 plaques
589 were not fluorescent. Crosses show mean titers, other symbols show individual mice. SC16
590 titers were greater than HSV-G in noses, greater than HSV-RG in TG, and greater than both
591 in skin, but the infections were otherwise equivalent. Specifically there was no difference
592 between HSV-RG and HSV-G.
593
594 **Figure 4. HSV-1 replicates in lysM$^+$ cells.**
595 **a.** Peritoneal macrophages or embryonic fibroblasts (MEF) of lysM-cre mice were infected
596 with HSV-RG (1 p.f.u./cell, 18h) then visualized by epifluorescence microscopy. >80% of
597 infected peritoneal macrophages were mCherry$^-$GFP$^+$; all infected fibroblasts were
598 mCherry$^+$GFP$^-$.
599 **b.** LysM-cre or C57BL/6 mice were infected i.n. with HSV-RG, or with MHV-RG as a positive
600 switching control (10^6 p.f.u. in 30µl under anesthesia). 1-2 days later lungs were assayed for
601 red / green switching by plaque assay. Circles show individual mice, dashed bars show
602 means. No switched virus was recovered from cre$^-$ C57BL/6 mice.
603 **c.** LysM-cre mice were infected as in **b**. 3 days later lungs and noses were assayed for red /
604 green switching by plaque assay. Circles show individual mice, dashed bars show means.
605 **d.** LysM-cre mice were infected i.n. with HSV-RG (10^6 p.f.u. in 30µl under anesthesia). 4 days
606 later organs were plaque assayed for total infectivity and red / green switching. Circles show
607 individual mice, dashed bars show means. Switching data were pooled from 2 experiments.
608 The % switching was not significantly different between noses, TG and skin.

609 **e.** LysM-cre mice were infected i.n. with HSV-RG (10^6 p.f.u. in 5µl). 4 days later organs were
610 plaque assayed for total infectivity and red / green switching. Circles show individual mice,
611 dashed bars show means. Switching data were pooled from 2 experiments. The % switching
612 was not significantly different between noses, TG and skin.
613 **f.** LysM-cre mice were infected as in **e**. 4 days later TG were stained for viral GFP and
614 mCherry. Neurons were identified by staining for βIII-tubulin. Nuclei were stained with DAPI.
615 Arrows show example fluorescent neurons.
616 **g.** LysM-cre mice were infected as in **e**. 4 days later skin sections were stained for viral GFP
617 and mCherry expression. Nuclei were stained with DAPI. Arrows show fluorescent cells in
618 the epidermis.
619 **h.** LysM-cre mice were infected by scarification of the whisker pad (WP) or the ear pinna
620 (EP) (10^6 p.f.u.). 4 days later organs were plaque assayed for red / green switching. DRG =
621 dorsal root ganglia. Data are pooled from 2 experiments. Circles show individual mice,
622 dashed bars show means.
623
624 **Figure 5. HSV-1 replicates in CD11c$^+$ cells.**
625 **a.** CD11c-cre mice were infected i.n. with HSV-RG (10^6 p.f.u. in 30µl under anesthesia). 3
626 days later lungs and noses were plaque assayed for red / green switching. Circles show
627 individual mice, crosses show means.
628 **b.** CD11c-cre or LysM-cre mice were infected i.n. with HSV-RG (10^6 p.f.u. in 5µl without
629 anesthesia). 4 days later noses and TG were plaque assayed for red / green switching. Circles
630 show individual mice, bars show means. In lysM-cre mice TG switching was less than nose
631 switching, but not significantly so ($p=0.08$). In CD11c-cre mice TG switching was significantly
632 less than nose switching ($p<10^{-5}$).

633 **c.** CD11c-cre were infected i.n. with HSV-RG (10^6 p.f.u. in 5µl without anesthesia). 5 days
634 later noses and TG were plaque assayed for red / green switching. Circles show individual
635 mice, crosses show means. TG switching was significantly less than nose switching
636 ($p<0.0005$).
637
638 **Figure 6. IFN-I limits HSV-1 infection of SSM.**
639 **a.** C57BL/6 mice were given IFNAR blocking antibody (αIFN) or not (cont) then infected i.f.
640 with HSV-GFP (10^6 p.f.u.). 1 day later footpads and PLN were plaque assayed for infectious
641 virus. Crosses show mean titers, other symbols show individuals. The dashed line shows the
642 lower limit of assay sensitivity. IFNAR blockade significantly increased PLN but not footpad
643 titers.
644 **b.** C57BL/6 mice were given IFNAR blocking antibody or not and infected i.f. with HSV-GFP
645 as in **a**. 3 days later virus titers were determined by plaque assay. Crosses show means,
646 circles show individuals. Dashed lines show assay sensitivity limits. IFNAR blockade
647 significantly increased all titers.
648 **c.** C57BL/6 mice were given IFNAR blocking antibody or not and infected i.f. with HSV-GFP as
649 in **a**. 1 day later PLN sections were analysed for viral GFP and antigen expression. Positive
650 cells were counted across 3 fields of view per section for 3 sections from each mouse.
651 Circles and squares show mean counts for individuals, bars show group means. IFNAR
652 blockade significantly increased GFP^+ and $antigen^+$ cell numbers.
653 **d.** Example images are shown for the mice infected in **c**. The left hand panels show low
654 magnification overviews, with viral GFP around the subcapsular sinus after IFNAR blockade
655 (arrows). The right hand panels show the relationship between viral GFP or antigen staining

(HSV-1) and the myeloid cell markers cell CD169 and CD68. Arrows show examples of co-localization.

e. C57BL/6 mice were given IFNAR blocking antibody then infected i.f. with HSV-1 SC16 (10^6 p.f.u.). 3 days later, PLN sections were stained for viral antigens plus markers of macrophages (CD169, CD68, F4/80), B cells (B220) and vascular endothelium (CD31). The images are representative of 3 mice per group. Arrows show examples of co-localization. CD169 staining was largely lost, but HSV-1 staining consistently co-localized with CD68 and F4/80, and not with B220 or CD31.

f. C57BL/6 mice were given IFNAR blocking antibody (αIFN), anti-NK1.1 depleting antibody (αNK) or no antibody (cont), then infected i.f. with HSV-GFP. 1 day later PLN were plaque assayed for infectious virus. Crosses show means, circles show individuals. The dashed line shows the lower limit of assay sensitivity. NK depletion significantly increased virus titers, but IFNAR blockade gave a significantly greater increase.

g. Mice were treated as in **f**, then assayed for infection 1 day later by counting viral GFP^+ cells on PLN sections (3 fields of view per section for 3 sections from each mouse). Squares show mean counts for individual mice, bars show group means. IFNAR blockade significantly increased GFP^+ cell numbers relative to controls. NK cell depletion did not.

Figure 7. IFNAR blockade increases HSV-RG replication in myeloid cells.

a. LysM-cre mice were given IFNAR blocking antibody (αIFN) or not (cont), then infected i.n. with HSV-RG (10^6 p.f.u. in 30µl under anesthesia). 3 days later lungs were plaque-assayed for total infectivity and virus switching. Crosses show means, circles show individuals. IFNAR blockade increased virus titers but not virus switching.

Journal of Virology

679 **b.** LysM-cre mice were given IFNAR blocking antibody or not, then infected i.n. with HSV-RG
680 (10^6 p.f.u. in 5µl without anesthesia). 3 days later noses and TG were plaque-assayed for
681 total infectivity and virus switching. Crosses show means, circles show individuals. IFNAR
682 blockade increased virus titers in both sites and virus switching only in TG.
683 **b.** LysM-cre mice were given IFNAR blocking antibody or not, then infected i.f. with HSV-RG
684 (10^6 p.f.u.). 3 days later footpads and PLN were plaque-assayed for total infectivity and
685 virus switching. Crosses show means, circles show individuals. IFNAR blockade increased
686 virus titers in both sites. After IFNAR blockade, PLN virus was significantly more switched
687 than footpad virus ($p<10^{-4}$). ND = not determined, due to insufficient plaque numbers.
688 **d.** CD11c-cre mice were treated, infected i.n. and analysed as in **a**. IFNAR blockade increased
689 virus titers in lungs but not virus switching.
690 **e.** CD11c-cre mice were treated, infected i.n. and analysed as in **b**. IFNAR blockade increased
691 virus titers in noses and TG and virus switching only in TG.
692 **f.** CD11c-cre mice were treated, infected i.f. and analysed as in **c**. IFNAR blockade increased
693 virus titers in footpads and PLN. After IFNAR blockade, PLN virus was significantly more
694 switched than footpad virus ($p<10^{-3}$). ND = not determined.
695
696 **Figure 8. Schematic diagram of HSV-1 host colonization and its relationship to myeloid**
697 **cells.**
698 This synthesis draws on the current paper and reference 5. The data are from mice but are
699 also consistent with what we know of human infection. (1) Incoming virions bind to
700 olfactory neuronal cilia. Neuronal infection provides a route across the epithelium. (2)
701 Infection does not spread to the olfactory bulbs, but rather to subepithelial tissues. Here
702 virions can enter trigeminal neurons directly; they can infect myeloid cells *en route*; or they

can enter lymphatics. At least 10% of virions recovered from TG had passed through a myeloid cell, and at least 25% if IFN-I signalling was blocked. (3) Virions reaching lymph nodes infect subcapsular sinus macrophages. IFN-I ensures that this infection is non-productive. Virus carried to LN in DC also seems not to spread. (4) Latency is established in the trigeminal ganglion. There is also acute infection spread between neurons, allowing exit via new sites such as the skin and oropharynx. (5) Virus delivery to the epidermis bypasses dermal myeloid cells.

Journal of Virology JVI Journal of Virology

Journal of Virology

JVI

Journal of Virology

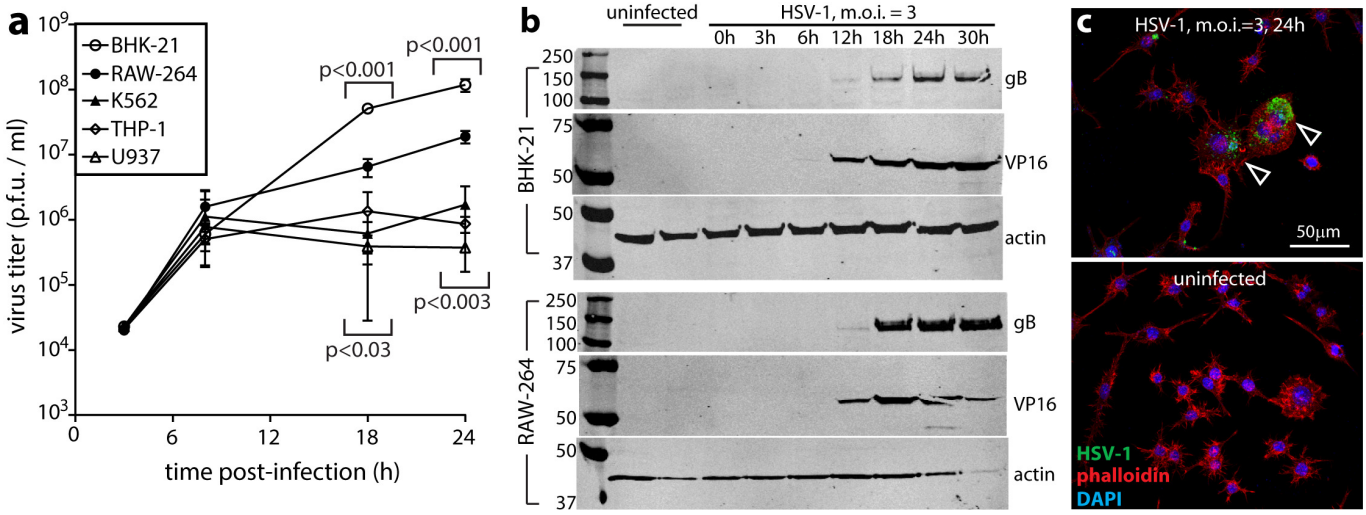

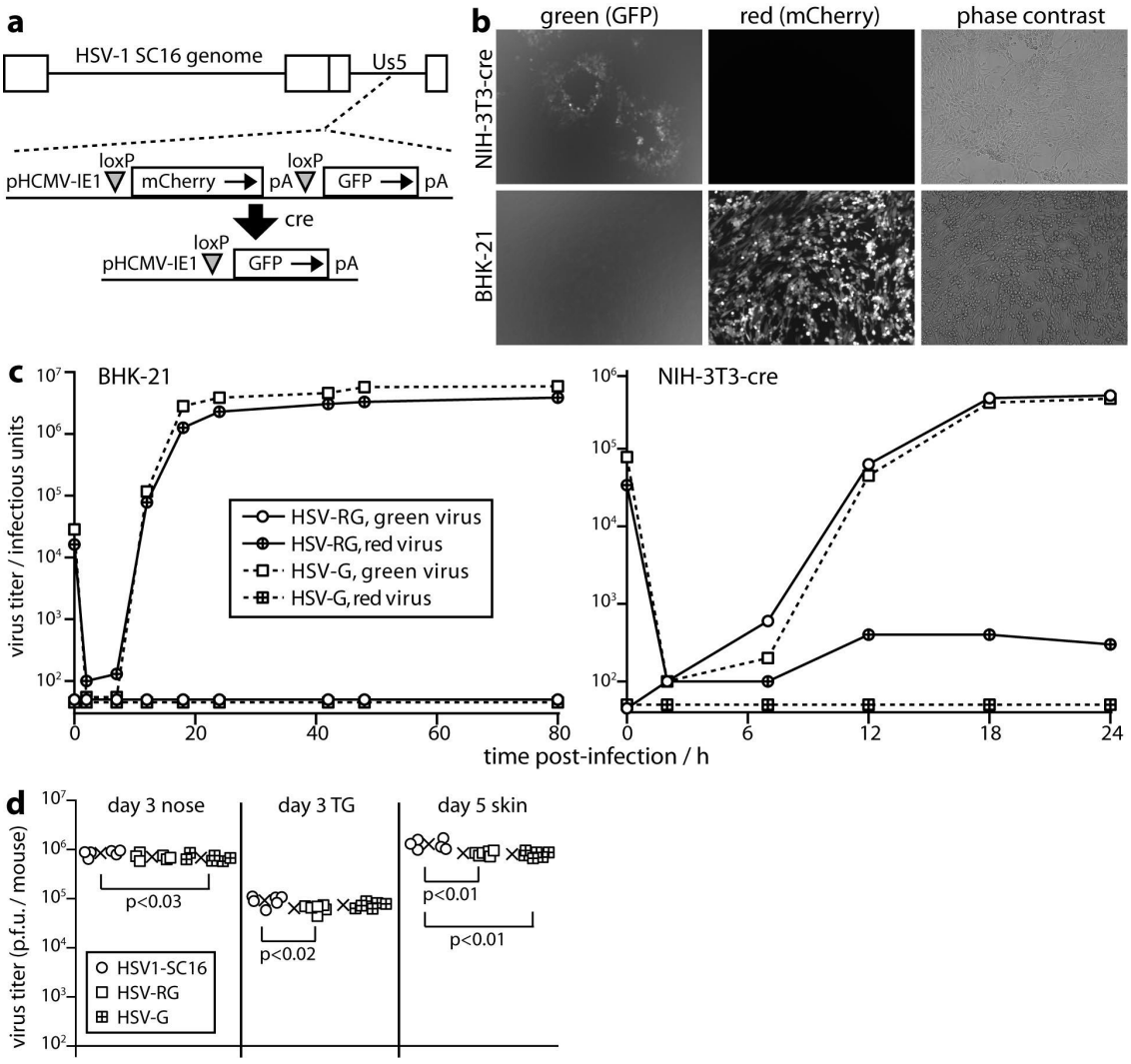

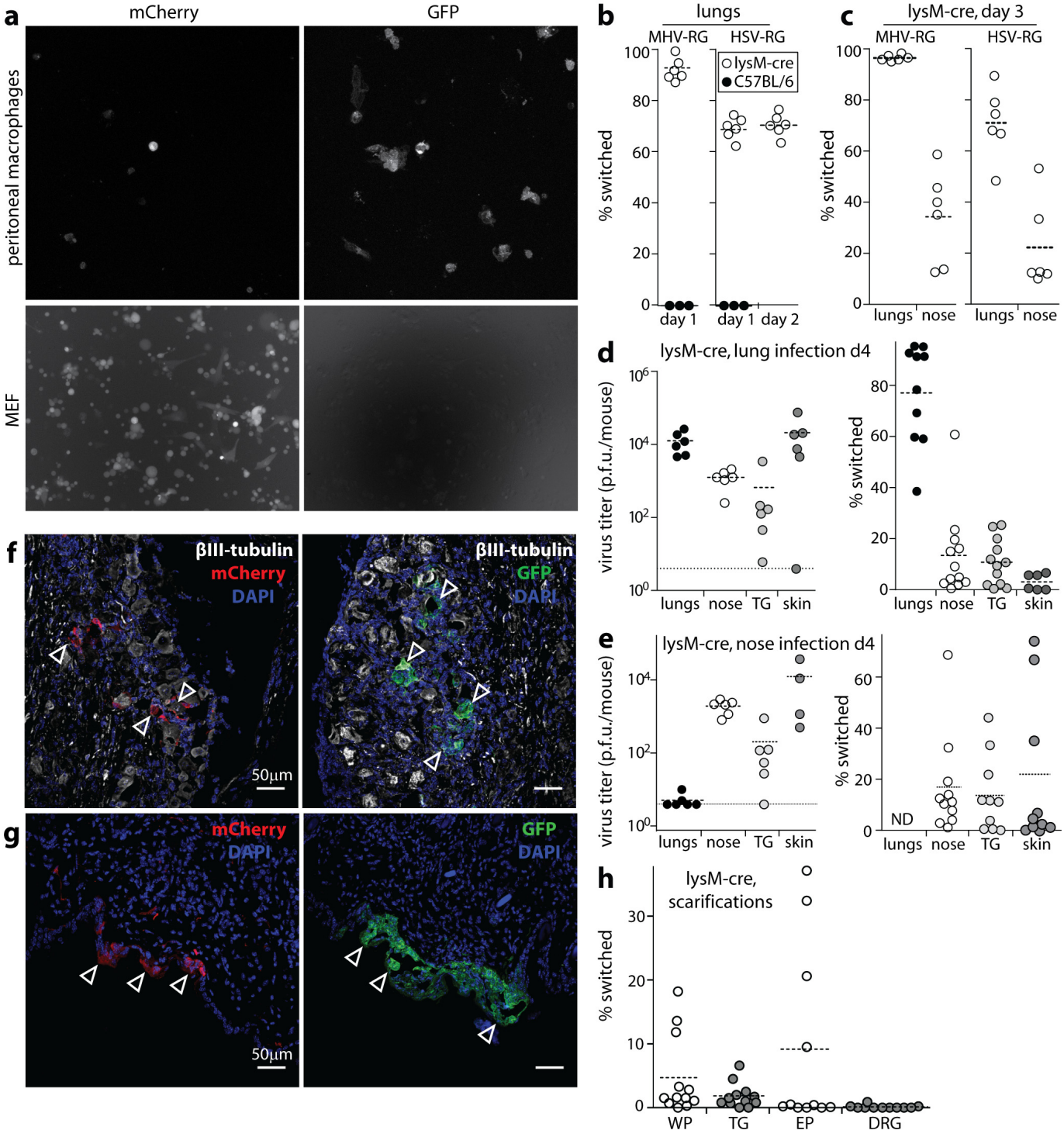

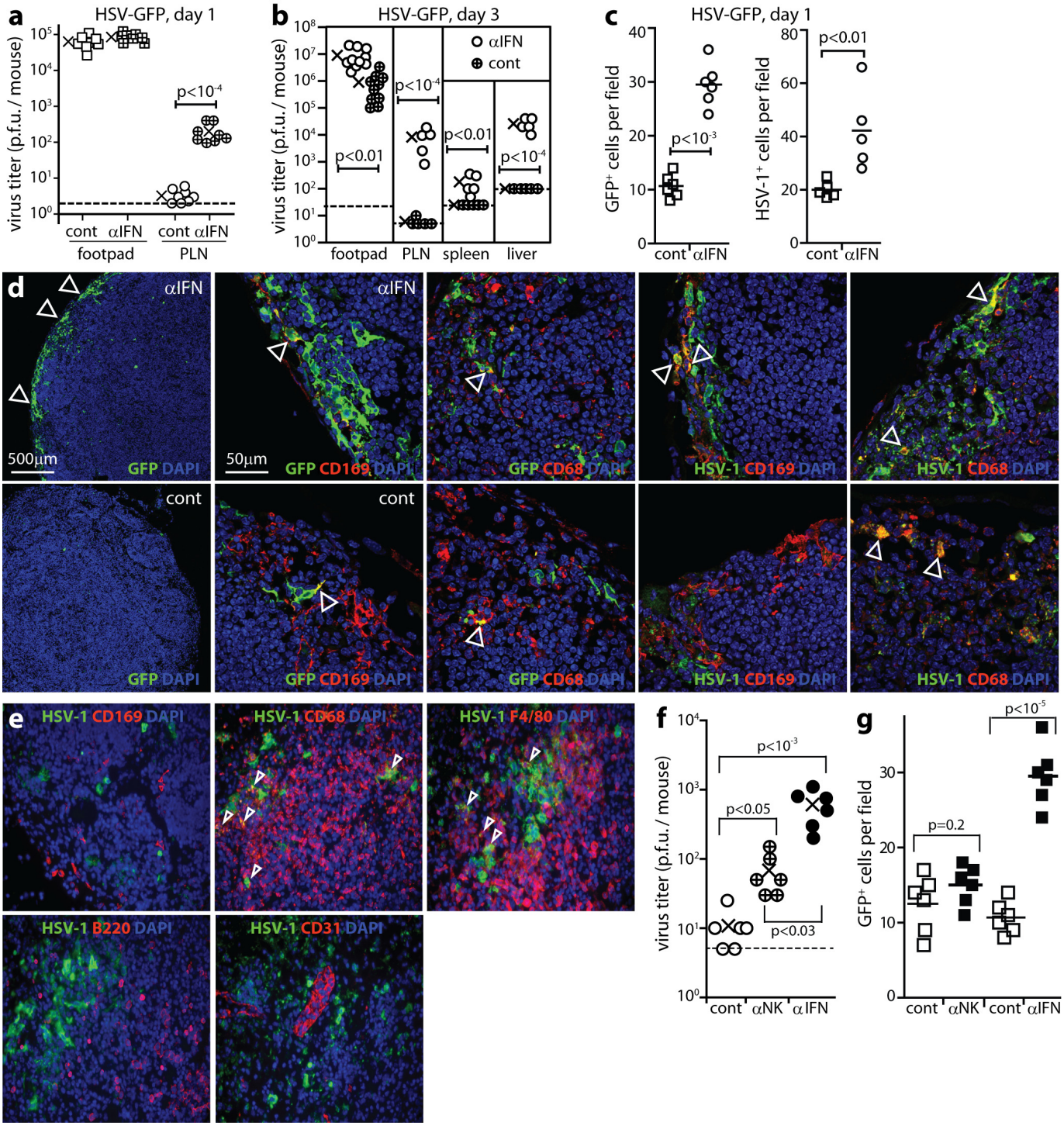

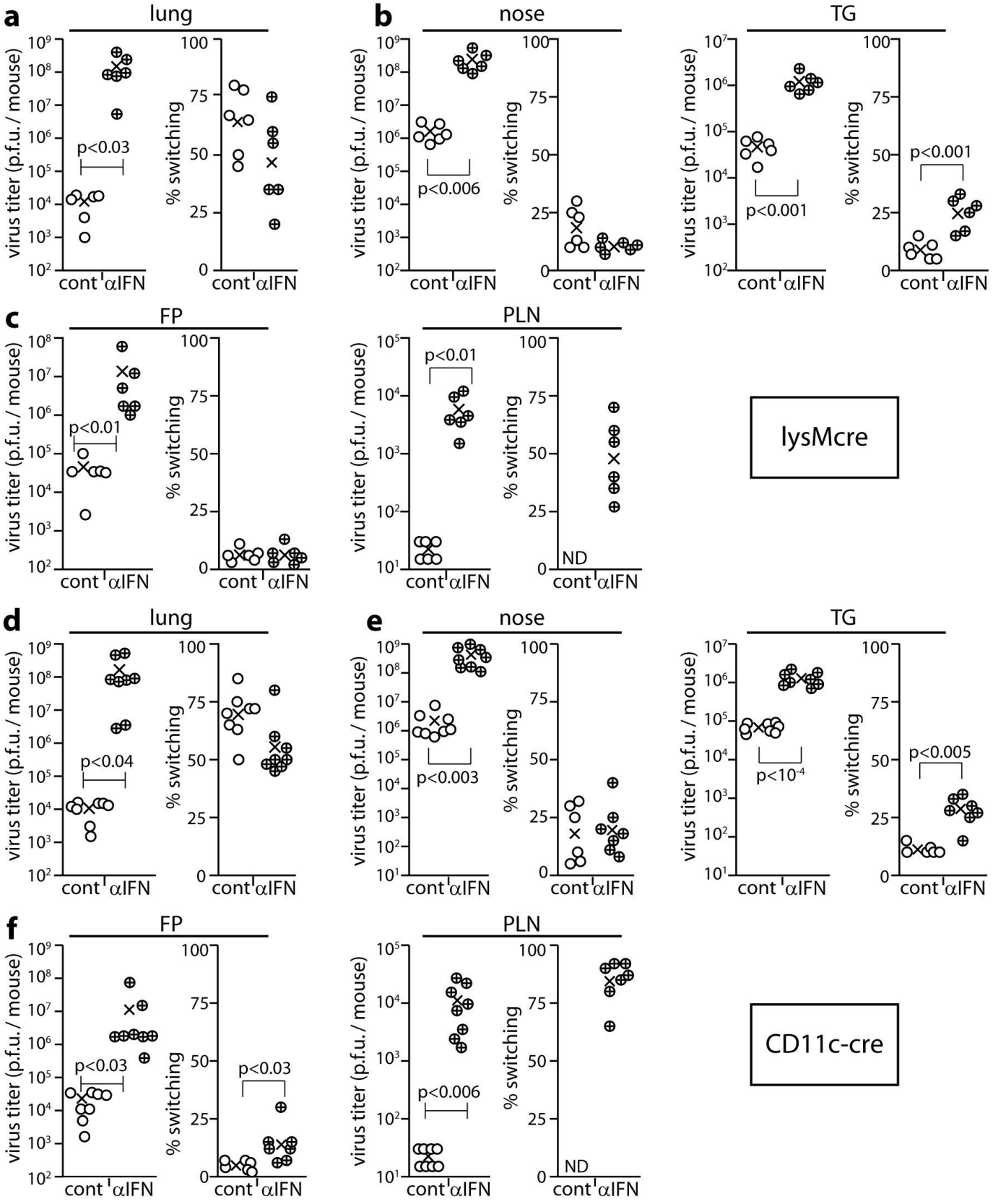

Journal of Virology